ITER collective Thomson scattering-Preparing to diagnose fusion-born alpha particles (invited)

Korsholm, S.B.; Chambon, A.; Gonçalves, B.; Infante, V.; Jensen, T.; Jessen, M.; Klinkby, E.B.; Larsen, A.W.; Luis, R.; Nietiadi, Y.

Total number of authors:
21

Published in:
Review of Scientific Instruments

Link to article, DOI:
10.1063/5.0101867

Publication date:
2022

Document Version
Peer reviewed version

ITER Collective Thomson Scattering – preparing to diagnose fusion-born alpha particles

S.B. Korsholm[1,a)], A. Chambon[1], B. Gonçalves[2], V. Infante[3], T. Jensen[1], M. Jessen[1], E.B. Klinkby[1], A.W. Larsen[1], R. Luis[2], Y. Nietiadi[2], E. Nonbøl[1], J. Rasmussen[1], D. Rechena[2], M. Salewski[1], A. Taormina[1], A. Vale[2], P. Varela[2], L. Sanchez[4], R.M. Ballester[4], V. Udintsev[5], and Y. Liu[5]

[1]*Technical University of Denmark, Department of Physics, 2800 Kgs. Lyngby, Denmark*
[2]*Instituto de Plasmas e Fusão Nuclear, Instituto Superior Técnico, Univ. Lisboa, 1049001 Lisbon, Portugal*
[3]*IDMEC, Instituto Superior Técnico, Univ. Lisboa, 1049001 Lisbon, Portugal*
[4]*Fusion for Energy, 08019 Barcelona, Spain*
[5]*ITER Organization, 13115 Saint Paul Lez Durance, France*

(Presented XXXXX; received XXXXX; accepted XXXXX; published online XXXXX)

The ITER Collective Thomson Scattering (CTS) diagnostic will measure the dynamics of fusion-born alpha particles in the burning ITER plasma by scattering a 1 MW 60 GHz gyrotron beam off fast-ion induced fluctuations in the plasma. The diagnostic will have seven measurement volumes across the ITER cross section, and will resolve the alpha particle energies in the range from 300 keV to 3.5 MeV; importantly, the CTS diagnostic is the only diagnostic capable of measuring confined alpha particles for energies below ~1.7 MeV and will also be sensitive to the other fast-ion populations. The temporal resolution is 100 ms, allowing capturing dynamics on that timescale, and the typical spatial resolution is 10-50 cm. The development and design of the in-vessel and primary part of the CTS diagnostic has been completed. This marks the beginning of a new phase of preparation to maximize the scientific benefit of the diagnostic, e.g. by investigating the capability to contribute to determination of the fuel-ion ratio and the bulk ion temperature, as well as integrated data analysis with other fast-ion and bulk-ion diagnostics.

I. INTRODUCTION

A. Collective Thomson Scattering diagnostics

Measurements of the dynamics of fast ions in a magnetically confined burning fusion plasma is important as well as challenging. In a burning fusion plasma, it is essential that the alpha particles born in the fusion reaction transfer a significant fraction of their energy to the bulk thermal ion population. The alpha particle birth energy is 3.5 MeV, while the bulk ion temperature in a burning plasma is around 20 keV. Hence, the alpha particle dynamics will differ significantly from that of the bulk ions, in that alpha particles are fast enough to interact with magnetohydrodynamic modes, such as the zoo of Alfvénic modes. Additionally, a burning plasma as that of ITER contains other fast ion populations due to the external heating required in order to reach fusion conditions. These are e.g. energetic ions from electromagnetic wave heating in the ion cyclotron range of frequencies (ICRH) or up to 1 MeV deuterons (D) from Neutral Beam Injection (NBI). Hence, in order to understand and optimize the operation of magnetically confined burning fusion plasmas it is important to be able to measure the fast ion populations and their dynamics as well as map out how they affect and are affected by plasma instabilities – such as sawteeth and Alfvénic modes.

[a)]Author to whom correspondence should be addressed: sbko@fysik.dtu.dk.

Collective Thomson Scattering (CTS) is one of the few fusion diagnostics that may provide spatially and temporally resolved measurements of the dynamics of confined fast ions in a burning plasma. The CTS principle is based on the scattering of an injected electromagnetic beam (typically in the mm-wave range) off the microscopic collective fluctuations in the electron distribution, caused by Debye-screening of the moving ions. These fluctuations are primarily due to the ion dynamics when observing at length scales greater than the Debye length, which is expressed in the Salpeter criterion[1]:

$$\alpha = \left(k^{\delta}\lambda_D\right)^{-1} > 1 \qquad (1)$$

where α is the Salpeter parameter, k^{δ} is the magnitude of the wave vector of the resolved fluctuations, and λ_D is the Debye length. The fluctuation wave vector k^{δ} is obtained from the matching condition $k^{\delta} = k^{s} - k^{i}$, where k^{s} is the known wave vector of the detected radiation and k^{i} is the known wave vector of the incident radiation. The Salpeter criterion sets linked requirements on the source frequency of the CTS

probing beam and the scattering geometry – the relative orientation of the injected probe beam and the so-called receiver beam acquiring part of the radiation resulting from the interaction between the probe beam and the microscopic plasma fluctuations. Typically, this results in a choice of probing frequency near the range of the electron cyclotron resonance of the plasma, and thus the scattering geometry is determined by quasi-optical transmission lines. For a detailed review of the CTS principle, one may refer to Refs. 2 and 3.

B. CTS diagnostics on current devices

Collective Thomson scattering diagnostic systems for measurements of both thermal ions and fast ions have been installed on several current and past tokamaks and stellarators. These include in chronological order of installation: TCA[4], W7-AS[5], JET[6,7], TEXTOR[8-11], ASDEX Upgrade[12-15], FTU[16], LHD[17,18], W7-X[19], and recently also HL-2A[20]. With the exception of the D_2O-laser probe at TCA[4], all the ion CTS diagnostics have been implemented using gyrotrons – typically in the frequency range from 77 GHz to 140 GHz, which matches the low-intensity ECE frequency range between the fundamental and the second harmonic electron cyclotron resonances.

While the CTS diagnostic has only matured over the past two decades[3,11], it has proven to be a useful and powerful diagnostic for measurements of confined fast ions – spatially resolved in the plasma core – bulk ion temperature and isotope ratios[21,22]. As the diagnostic operates at wavelengths of typically 2-5 mm, the in-vessel and plasma facing components are robust and relatively resilient to the harsh conditions in a burning plasma device. Thus, the development and implementation of the CTS diagnostic on ITER has a significance for future fusion reactors such as DEMO, in parallel to its imminent importance for the better understanding of ion dynamics in the ITER burning plasma.

C. Background of the ITER CTS diagnostic

The first ITER reference design did not include a Collective Thomson scattering diagnostic. At the same time, the ITER diagnostic suite did not cover well the fast ion measurement requirements. Hence, starting in 2003 EFDA[23] funded a feasibility study for a fast-ion CTS diagnostic for ITER. Multiple probe frequency options were investigated (CO_2, D_2O, 170 GHz gyrotron, and 60 GHz gyrotron), and it was found that the best signal-to-noise and also most robust diagnostic should operate at a probe frequency of 60 GHz delivered by a ≥1 MW gyrotron[24-29]. This frequency is below the fundamental electron cyclotron resonance of ITER at nominal magnetic field of $B_t = 5.3$ T. This poses a specific challenge that we return to in Section II. The feasibility study confirmed that the 60 GHz ITER CTS diagnostic would be able to contribute to fast ion measurements including:

- Alpha density profile
- Alpha energy spectrum
- p, D, T, ^{3}He Energy Spectrum

Following the feasibility study, the fast-ion Collective Thomson Scattering diagnostic was included as an *enabled* diagnostic in the 2007 ITER Baseline, meaning that the in-vessel CTS front-end is part of the ITER construction budget. The European Domestic Agency Fusion for Energy (F4E) is responsible for the development, design, and delivery of the in-vessel CTS front-end components, as well as for providing the functional specifications of the remaining parts of the diagnostic system. In 2014 the DTU/IST Consortium[30] initiated the design and development under a framework contract with F4E[31], and the analysis, development, and design of the system is now complete. This paper summarizes the main features of this diagnostic, as well as the analysis and considerations leading to this design. Note that the paper only describes the in-vessel part of the CTS diagnostic, since the ex-vessel parts, including the vacuum windows, are being developed by other parties.

D. Outline of the paper

Section II provides an overview of the diagnostic design, including a review of the design principles driving the development of the fast-ion ITER CTS diagnostic system. The section also describes some of the critical components of the diagnostic. The predicted diagnostic performance of the CTS diagnostic is described in Section III, followed by brief reviews of the neutronics analysis (Section IV), the Reliability analysis (Section V), and the remote handling and maintenance assessment (Section VI). The development of the CTS diagnostic has been supported by prototyping as described in Section VII. Finally, the summary and outlook can be found in Section VIII.

II. OVERVIEW OF THE DIAGNOSTIC DESIGN

The development and design of the ITER CTS diagnostic has been requirement driven; aiming at fulfilling the measurement requirements to the extent possible while balancing against the many technical, engineering, and operational requirements[32]. These requirements are increasing in importance and complexity when designing diagnostic systems for a burning plasma device as ITER, and can hardly be compared to the requirements of present devices. As an example, one may consider the balance between the diagnostic performance optimization requiring a larger aperture in the plasma facing diagnostic first wall against the requirements on acceptable radiation levels in the port cell area – levels flowed down from requirements from the French Nuclear Authorities. The neutronics modeling on the impact of the CTS system design has thus been an important support to the diagnostic development, and more on the topic can be found in Section IV.

The requirements and boundary conditions of the in-vessel front-end of the CTS system included e.g. (besides the neutronics requirements): all components should be located in the drawer #3 (diagnostic port plugs are divided into three mechanically independent drawers – having the full height and depth of the port plug, and one third of the width) of the equatorial port plug #12 (EPP12), no mechanically moveable components, all components and their fixtures should be able to withstand steady state and intermittent loads from nuclear, thermal, electromagnetic, and seismic events throughout their lifetime, the materials and coatings used for the components should be on the approved ITER list of materials, and all remote handleable components should enable remote maintenance in the Hot Cell Facility (HCF).

The CTS diagnostic is the only diagnostic assigned to the diagnostic shield module (DSM) of drawer #3, leaving more freedom for the system configuration. Nevertheless, careful attention had to be payed to the interfaces between the components and associated cutouts to the cooling water pipes, shielding modules, electrical wiring and other infrastructure of the DSM.

A. System outline

The final design of the in-vessel components of the ITER CTS diagnostic in EPP12 drawer #3 can be seen in FIG. 1. The vacuum vessel boundary is the EPP12 closure plate (not shown) to the right in the picture. The gyrotron probe beam is transmitted from the gyrotron in the Assembly Hall to the tokamak building through a transmission line with circular corrugated waveguides. At the closure plate the gyrotron probe beam is coupled through a single-disc diamond window via a two-mirror quasi-optical coupling system on either side of the window. The upper part of the in-vessel CTS system is the launcher system; and the gyrotron probe beam after the diamond window can be seen entering (1) the blue launcher "bucket" in the top right. The latter is an enclosure included in the design to reduce the level of stray light on the remaining parts of the system and DSM. The bucket supports the two coupling mirrors, which couple the beam from the window

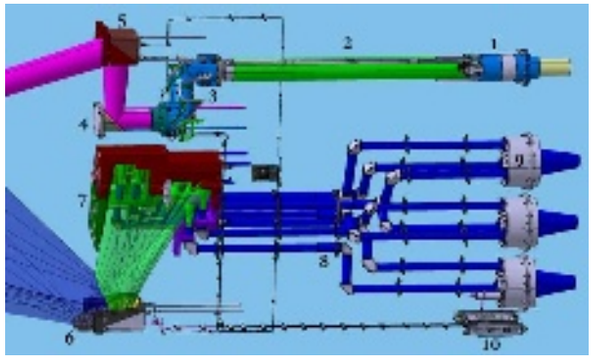

FIG. 1. The CTS system in-vessel front-end components. The annotations of key components are described in the text.

into (2) a 1400 mm circular corrugated waveguide (Ø 88.9 mm inner diameter). The waveguide – which is described further in subsection II.C.1 – is connected to a sliding joint allowing for longitudinal displacements due to thermomechanical stresses. The gyrotron probe beam is transmitted via (3) a unit consisting of circular corrugated waveguides and two miter bends, after which the beam has a free-space propagation via two quasi-optical mirrors (4+5), launching the probe beam (shown in purple in FIG. 1) in the desired (and fixed) direction into the plasma. The double miter bend unit was used to create a so-called dog-leg in order to reduce the direct streaming of neutrons from the plasma through the port-plug.

As a consequence of the requirement of no moveable components, the receiving quasi-optics have been arranged so that the gyrotron probe beam is intersected by seven receiver beams. Each of these receiver beams is defined by the combination of the opening of the receiver circular corrugated waveguide (Ø 31.75 mm inner diameter; blue in FIG. 1), (7) the dedicated mirror M3 (machined into the M3 mirror cassette; brown and green), and (6) the common plasma-facing receiver mirror M2 in the bottom left part of the drawer. The receiver beams are seen in green and blue. The setup enables simultaneous measurements in seven scattering volumes distributed across the plasma cross section (see more in Section III). The received radiation is transmitted via (8) the waveguides and miter bends (dog-legs) towards the closure plate, where it couples through fused-silica vacuum windows in groups of three via (9) a two-quasi-optical mirror setup similar to that of the gyrotron transmission line. The grouping of receiver beams is explained further in subsection II.C.2.

On the ex-vessel side of the closure plate, the receiver beams are coupled into a waveguide transmission line leading to the Diagnostic Building, where the CTS receiver electronics and data acquisition cubicles are located. There is a total of nine transmission lines between the EPP12 and the Diagnostic Hall. Besides the seven receiver beams covering the plasma cross section, it was deemed advisable to have a so-called passive view receiver, which is similar to the other seven receivers, but with no intersection of the gyrotron probe beam. This will help monitoring the background radiation and detect any unforeseen interaction between the gyrotron probe beam and the plasma. Such a passive view has proven very useful in the interpretation of fast-ion CTS data on ASDEX Upgrade[15]. The ninth transmission line is used for calibration and monitoring of the gyrotron beam and is described in subsection II.C.3. The fundamental waveguides from these systems are seen as fundamental waveguides in FIG. 1, and (10) is the auxiliary box enabling the calibration and monitoring systems.

Besides these key components, the in-vessel CTS design also contains active cooling of the launcher line components and the plasma-facing components plus a total

of 13 thermocouples monitoring the temperature of the CTS components.

B. Consequence of operating frequency

The probe frequency of 60 GHz was chosen in order to reduce the ECE background radiation and maximize performance[24,25]. The frequency range of interest around the probing frequency depends on the Doppler shift of the radiation scattered due to the fusion-born alpha particles, which corresponds to ≲±5 GHz for the chosen scattering

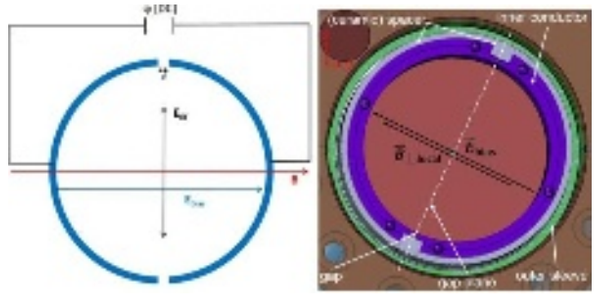

FIG. 2. The SBWG bias circuit (left) and cross-section of the ITER CTS SBWG (right). The ITER CTS SBWG bias circuit will operate at voltages up to ±1 kV.

geometry. Hence, the relevant frequency range for the fast-ion ITER CTS diagnostic is 55 to 65 GHz, and recent studies and modeling have shown the ECE levels (noise in the CTS analysis) to be very low in ITER at frequencies below 65 GHz[33].

Operation at 60 GHz means that the diagnostic must be operated in X-mode, since the O-mode cutoff is at the edge of the plasma. At the same time, the frequency range is close to X-mode cut-off, leading to significant refraction of both the probe and receiver beams. However, the refraction acts such that a significant intersection between the probe and receiver beams is still ensured, though in radial locations different from those of vacuum beam tracing. The refraction is highly dependent on the plasma scenarios – particularly the density profile – and hence the spatial resolution and positions of the CTS measurements depends on the chosen scenario.

The choice of a sub-fundamental probe frequency leads to a critical challenge, namely that the probing beam passes the fundamental electron cyclotron resonance inside the port plug – an issue we describe in the next subsection.

C. Critical design elements

The system layout of the CTS diagnostic was described above, and in this section we describe some more details of some specific and/or critical components.

1. Split biased waveguide

The critical issue of transmitting a 1 MW gyrotron beam through the fundamental electron cyclotron resonance inside an ITER port plug has required due and specific attention. The fundamental resonance in a magnetic field B, is found where $\omega = eB/m_e$, where e is the electron charge and m_e is the electron mass. According to the total magnetic field maps of ITER, the 60 GHz resonance will be located at $R \approx 10.4$ m for the ITER reference magnetic field of 5.3 T (on-axis), i.e. the resonance is inside the EPP12. In case a sufficient neutral gas pressure builds up in the port plug, there is a risk that a random ionization may initiate a cascading ionization of the gas in the waveguide. This may be driven by the electric field in the gyrotron beam, and even worse, after a plasma is created at the resonance a non-negligible fraction of the 1 MW gyrotron beam may be absorbed in a narrow region. This would lead to a catastrophic failure of the launcher waveguide and likely a leak of the cooling system forcing a halt to ITER operation. Consequently, this is a risk that has to be mitigated.

The solution chosen to mitigate this is the design of a longitudinally-split electrically-biased waveguide[34] (SBWG). The design is based on a concept proposed and used on DITE and DIII-D[35], where a bias voltage is set up across two electrically isolated halves of the circular corrugated waveguide (See FIG. 2). The bias voltage will cause any free electrons to diffuse to the anode before they cause an ionization cascade. Historically, the concept was used with success, though on smaller devices and lower powers. While a full-scale prototype (including a 60 GHz 1 MW gyrotron) would be unfeasible, Particle-in-Cell simulations of the effectiveness of the SBWG mitigation have been performed[36] – initially reproducing the historical experimental results - for reference. In conclusion from the modelling, the operational limits of the ITER CTS gyrotron for an SBWG bias circuit voltage of ±1 kV is a neutral pressure in the EPP12 of ≤ 20 Pa. The neutral pressure during an ITER plasma pulse will initially be much lower, but no predictions exist for the neutral pressure over time. Consequently, the neutral pressure in the ports should be monitored and the CTS gyrotron operation should be stopped in case the pressure approaches the limit. As a side note, the bias circuit should also be used as a monitor of the breakdown prevention, since a significant change (dI/dt) in the current drawn (it should normally be low) would indicate that the SBWG is presently preventing a plasma breakdown.

2. Quasi-optical closure plate coupling systems

The connection between the in-vessel and ex-vessel parts of the CTS system is restricted by the allotted area of the EPP12 closure plate. A further restriction is the required space reservations for inspection and maintenance around the standardized ITER vacuum window assemblies. This severely reduced the number of receiver transmission lines that could be fitted.

In an effort to make maximum use of the area, it was decided to use the largest available windows (clear aperture of Ø160 mm) – double disc fused silica. By the arrangement

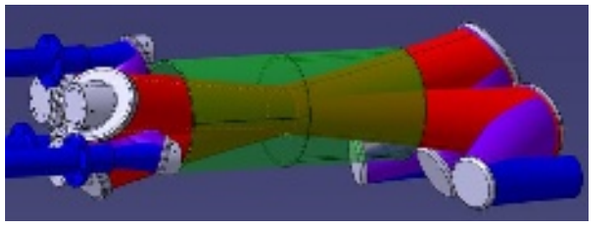

FIG. 3. The configuration of the CTS receiver beams at the closure plate coupling system. The green cylinder represents the window assembly "tunnel" through the closure plate.

seen in FIG. 3, it is possible to fit three receiver beams through each window, making a total of nine transmission line connections between the in-vessel system and the diagnostic building cubicles. The transmission from the in-vessel to the ex-vessel waveguide transmission lines are ensured by a two-quasi-optical mirror system on either side of the window assembly – as for the gyrotron beam coupling. In order to reduce sensitivity to stray radiation, the receiver coupling systems are located in an enclosure (a "bucket"), which supports the three times two mirrors and ensures the associated alignment of the waveguides.

3. Calibration and the auxiliary monitoring system

The preceding sections describe how the seven CTS receiver lines and the passive view occupy eight of the nine transmission lines. The last transmission line is used as an auxiliary transmission line for (1) monitoring the gyrotron performance via connection to a sniffer probe in the second miter bend of the probe transmission line, and (2) calibration and alignment verification of the receiver transmission lines. The former is done during plasma and gyrotron operation – based on signals transmitted from the tokamak to the diagnostic cubicles, while the latter is done between ITER plasma pulses – using a calibration signal transmitted from the diagnostic cubicle to the in-vessel system. The auxiliary transmission line can thus be used for two independent purposes. This is possible due to the passive and linear microwave circuit installed in the so-called Auxiliary Box in the lower right part of the port plug drawer #3 as seen in FIG. 1 (10). The circuit basically consists of two orthomode transducers and two directional couplers.

The in-vessel receiver quasi-optics and transmission lines will routinely be subject to a relative calibration. An ex-vessel broadband tunable (55-65 GHz) microwave signal will be transmitted from the diagnostic cubicles via the auxiliary transmission line. And further via the in-vessel auxiliary box and a fundamental circular waveguide, the signal will emanate from a small Ø3.581 mm opening in the center of the M2 mirror. The microwaves will be coupled into all the receiver and passive view transmission lines and back through the in- and ex-vessel transmission lines to the receiver electronics. This in-situ test will be performed on the newly installed system and will frequently be repeated between plasma pulses, so as to monitor the relative performance of the individual transmission lines against their initial benchmark measurements.

The calibration, alignment, and monitoring system of the ITER CTS diagnostic will be described in detail in a separate forthcoming publication.

D. Functional tolerances

Following component manufacturing, assembly, installation, and not least due to thermal loads during plasma operation, it is very likely that the spatial location of the ITER CTS components will deviate from the as-designed ideal locations. In order to establish the range of acceptable functional tolerances, the effect of this was modelled using a Monte Carlo method.

A Monte Carlo simulation was required, as each of the CTS front-end components would be able to translate in three directions and rotate in three directions independently of each other. In order to simulate the worst case scenario, each component was assigned a perturbation in each of the six parameters with an amplitude of random size, within a limit defining the maximum range of the perturbation. This limit was ultimately the quantity of interest, since this defined the acceptable range that the component could deviate from the as-designed location. The assessment of whether the collective (and independent) misalignments in one Monte Carlo iteration were acceptable relied on their impact on diagnostic performance, which is quantified by the degradation in the overlap factor as figure of merit (see Section III).

The tolerance analysis revealed the CTS front-end to be relatively robust against misalignments, and accounting for only the front-focusing quasi optics (i.e. the components in the left most part of FIG. 1.), the acceptable range in each of the three spatial dimensions is $\leq\pm 3$ mm and rotational misalignments of $\leq\pm 0.2°$. The sensitivity of the coupling quasi-optics near the closure plate is a little higher. While manufacturing, assembly, and installation (using alignment pins to the DSM) should not result in larger deviations from the ideal locations, the thermomechanical deformations of the DSM and CTS components during operation can amount to ~1 mm in any direction. However, this is still within the acceptable limits and the analysis indicates that the CTS diagnostic will perform as required.

III. PREDICTED PERFORMANCE OF THE FAST-ION ITER CTS DIAGNOSTIC

Optimizing the diagnostic performance of the ITER CTS diagnostic while fulfilling the technical requirements has been the driving aim throughout the development of the diagnostic. The extensive performance analysis for the

ITER CTS diagnostic is described in reports and highlighted in a number of publications[27-29,37,38]. Here, it will suffice to summarize the spatial resolution and the fulfillment of the measurement requirements.

The spatial resolution of the ITER CTS system is defined as the radial extent of the scattering volumes resulting from the overlap between the gyrotron probe beam and the individual receiver beams. The location and radial extent of these overlap volumes are shown in FIG. 4 for the ITER baseline and steady-state plasma scenarios (central density n_{e0} = 1.0 10^{19} m^{-3} [33] and 6.0 10^{19} m^{-3}, respectively). Each of the colored ellipses represents the volume from which 75% of the scattering signal originates. Comparison between the two plasma scenarios illustrates how the plasma density profile affects the beam propagation – and with that the spatial resolution. Nevertheless, we find that for the baseline scenario, the spatial resolution ranges from 6 to 115 cm, with the resolution in the core being 59 cm. For the steady-state scenario, the corresponding values are 18 to 56 cm, with 36 cm in the core.

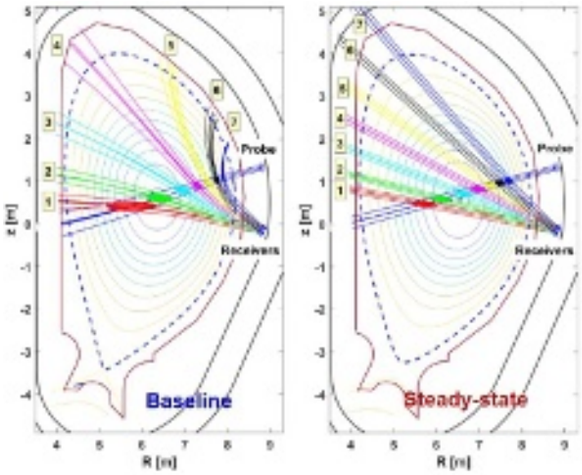

FIG. 4. The location and size of the CTS scattering volumes across the ITER plasma cross-section for the Baseline (I =15MA) and Steady-State (I=10MA) scenarios. Ellipses outline the extent of each scattering volume, defined here as the region containing 75% of the scattering signal.

TABLE I. The performance assessment of the ITER CTS diagnostic[37]. The required accuracy is 20%. P_b is the conservative ECE background level at the relevant frequencies.

Measurement parameter	Range	Time resolution	Inferred accuracy
Alpha density profile at $n_\alpha>10^{17}$ m^{-3}	-	100 ms	9±2% (baseline scenario, P_b=100 eV)
			8±2% (steady state scenario, P_b=1 keV)
Alpha energy spectrum	E = 0.3-3.5 MeV	100 ms	Spectral shape assumed in all inversions
P, D, T, ^{3}He energy spectrum	E = 0.1-1 MeV	100 ms	3% (baseline scenario, P_b=100 eV)
			17% (steady state scenario, P_b=1 keV)

The general procedure for assessing the accuracy with which fast-ion densities can be inferred with the ITER CTS consists of generating synthetic ITER CTS data in the presence of background noise, frequency-dependent refraction, systematic uncertainties, and uncertainty on auxiliary plasma parameters. This is followed by Bayesian inversion of the modelled spectra to recover the underlying fast-ion parameters.

Based on such trial fits to synthetic spectra, performed as described in Ref. 37, we find that the spatial density profile of alpha particles can, on average, be constrained to within ~10% and 15% at 100 ms time resolution for the ITER baseline and steady-state plasma scenarios, respectively. This applies to all receivers probing plasma locations, corresponding to alpha densities $n_\alpha > 10^{17}$ m^{-3}, as set forth in the measurement requirements. The corresponding accuracies for the fast-D density profiles are ~5% and ~15%, respectively. Hence, these accuracies all remain below the required 20% as seen in TABLE I.

The ITER measurement requirements on specific parameters are not generally restricted to individual diagnostics but can be achieved by integrated data analysis of several diagnostics. The CTS measurements at ITER will be analyzed together with gamma-ray spectroscopy measurements[39]. The integrated data analysis of these diagnostics will allow velocity-space tomography of the 2D fast-ion velocity distribution function in the plasma center[38]. The alpha particle energy spectrum can then be derived by integration of the 2D velocity distribution function over the pitch – See FIG. 5. However, as gamma-ray spectroscopy is not sensitive to alpha particles at energies below 1.7 MeV, this analysis will only provide the energy spectrum above 1.7 MeV. Techniques for inferring energy spectra based on CTS measurements alone, which are sensitive down to about 300 keV, require additional prior information, such as isotropy[40].

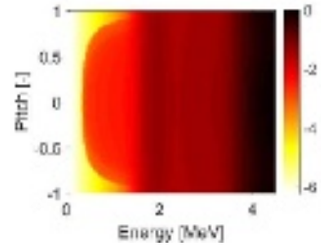

FIG. 5. Illustration of the gross velocity-space sensitivity of CTS and GRS together. (E; p) are the energy and the pitch of the particles. Reproduced with permission from Nucl. Fusion **58**, 096019 (2018). Copyright 2018 IOP Publishing Ltd.

IV. NEUTRONICS ANALYSIS

The neutronics analysis of the in-vessel CTS system and the modifications to the blanket modules and the diagnostic shield module (DSM) drawer #3 (e.g. cut-outs

and apertures for the components and the microwave beams) has closely accompanied the development of the design. The purpose has been to determine if modifications done for diagnostic performance reasons would violate the requirements on the shutdown dose rates (SDDR) at the equatorial port plug closure plate in the port interspace for hand-on maintenance purpose[41-43]. By requirement, the dose level in the ports cells, where hands-on maintenance is planned, should not exceed 100 μSv/h 10^6 seconds (~12 days) after shutdown. The neutronics analysis has also assessed the nuclear loads on the CTS components and thus served as one of the inputs to the thermomechanical analysis of the system[44].

During the Final Design Phase the neutronics analysis was repeated in order to demonstrate that the updated design remained compliant with the requirement that the dose rate in the port interspace does not exceed those of the reference design, according to the radiation safety ALARA (as low as reasonably achievable) principle. The analysis also modelled the neutron and gamma fluxes and heat loads on the final design CTS components as well as the displacements per atom (dpa). The nuclear analysis was performed using the Monte Carlo code D1S-UNED v3.1.4, along with the cross-section library FENDL 3.1 c/d for neutrons and MCPLIB84 for photons that belong to the currently accepted codes and data libraries for ITER nuclear analyses.

The neutronics load on the CTS components was found to be largest on the large plasma-facing collective receiver mirror (M2) in the lower part of the port-plug. On M2, the local peak value reaches 2.6 W/cm^3, and the total power deposited is 13.2 kW, underlining the need for active cooling. In relation to radiation damage, M2 also suffered the most of all components with 1.68 dpa per full power year of plasma operation.

The analysis also confirmed that the present design of the CTS system remains compliant with the radiation safety requirements, and that from the neutronics point of view, no further design optimization of the CTS system is needed[43].

V. FUNCTIONAL ANALYSIS AND RAMI ANALYSIS

The CTS diagnostic is required to be available for measurements during ITER operations at a minimum of 97% after 20 years of ITER operation, and the CTS system itself should have virtually no impact on the overall ITER operation. The verification of the fulfillments of these requirements is carried out using a so-called RAMI analysis[45] (Reliability, Availability, Maintainability, and Inspectability). This analysis is preceded by a functional analysis of the full system and the interaction between the functionality of the different components of the diagnostic. Subsequently, a Failure Modes, Effects and Criticality Analysis (FMECA) is performed[46], considering the identification of the failure modes based on the functional analysis of the system, as well as a qualitative assessment of the causes and effects on the functions of the system, on the system itself and on the operation of the ITER machine. In addition, the analysis also considered quantitative assessment of the *Occurrence* of the causes and of the *Severity* of the effect and the prioritization in *Minor*, *Medium*, and *Major Risks*, as a function of the *Criticality* of all failure modes in a *Criticality Matrix*. The functions, failure modes, consequences and impact on the ITER operation were defined. The severity and occurrence of each failure mode was determined for each component. The duty cycle, failure rate, Mean Time Between Failure (MTBF), and Mean Time To Repair (MTTR) for each failure mode was also defined and served as a basis for recommending mitigation actions such as increased monitoring by thermocouples and monitoring of coolant parameters, as well as ensuring an interlock on gyrotron operation if the operation of the above-mentioned SBWG fails.

The FMECA was succeeded by the Reliability Block Diagram (RBD) modelling and simulation of the complete in-vessel front-end of the CTS diagnostic[47]. A series of simulations was done taking into account e.g. that not all receiver views need to be available in order to have a useful diagnostic, and also that measurements may be useful without the passive view receiver. For the critical requirement (97%) on the availability of the full launcher/probe system as well as the primary receiver mirror M2, the simulations showed an availability of 97.65% after 20 years of ITER operation. Regarding the impact of the CTS front-end on ITER operations, the mean availability of the ITER operations (considering the failure of the front-end CTS components alone) is estimated to be of 99.995%.

While the FMECA and RBD simulations have contributed to focusing the efforts towards the most critical components and processes, the final assessment has demonstrated the compliance with the availability requirements. This, in turn, classifies the CTS front-end components as Remote Handling Class 3 – see Section VI.

VI. REMOTE HANDLING AND MAINTENANCE

The ITER CTS front-end has been classified as remote handling class 3 (RHC3), based on the RAMI analysis. This means that the CTS components "are not expected to require remote maintenance during the lifetime of ITER, but their failure would impact ITER operation. Components which have a failure probability less than 1 in 200 years but greater than 1 in 2000 years (based on RAMI analysis) should be RH Class 3. Although these components must be designed to make disassembly and repair/replacement feasible by remote handling means, their design emphasizes the reliability and performance optimization. Maintainability must be verified by detailed RH assessment"[48].

Based on the RAMI analysis and agreements between F4E and the ITER Organization, all water-cooled components (except for the M3 mirror cassette) needs to be remote handleable in the HCF if maintenance is unexpectedly required. In order to interface the CTS components with the manipulator tools and cranes in the HCF, dedicated remote handling (RH) brackets were designed. They feature a mushroom-type protrusion that will act as the interface to the gripper of the tool in the HCF.

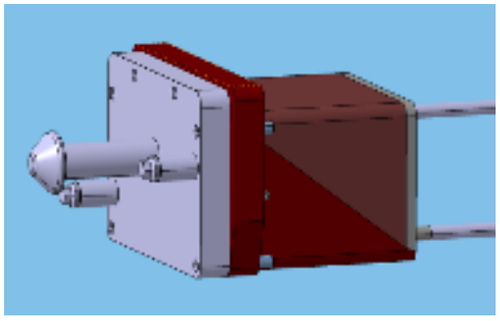

FIG. 6. The RH bracket mounted on Mirror 1 – the plasma facing launcher mirror. The plate captivates the mounting bolts of M1.

The RH brackets also feature a plate into which the bolts of e.g. the mirrors will be captivated after unbolting them. An example of the bracket for Mirror 1 is shown in FIG. 6.

The Remote Handling Compatibility Assessment has been performed along with the associated series of Task Definition Forms detailing which actions to be performed in the HCF during remote handling maintenance of a given CTS component. The conclusion is that with the current Final Design of the CTS front-end and the designed RH brackets, the CTS system is compatible with the requirements in the ITER HCF.

VII. PROTOTYPE TESTING

The development of the CTS diagnostic has been accompanied by a number of prototype tests of individual components, subsets of the system, or more functional tests[49]. It has not been within the scope to make a full scale mock-up of the complete CTS front-end, but the tests that have been performed have consolidated the design. In the phases following manufacturing, specific and detailed Factory and Site Acceptance tests have been defined. Prior to installation in the ITER vacuum vessel, the CTS system has to undergo a multi-day diagnostic functional test in the Port Plug Test Facility on the ITER site.

VIII. SUMMARY AND OUTLOOK

We have reviewed the key features, potential, and associated analysis of the ITER fast-ion CTS diagnostic that has passed the Final Design Review in late 2021. The next steps towards implementation and operation at ITER will be manufacturing of the diagnostic system by a supplier to Fusion for Energy, followed by delivery to the ITER site. The CTS system will be installed in the equatorial port plug #12, and after alignment, calibration, and beam characterization in the ITER Port Plug Test Facility, the port plug will be installed in the ITER vessel. Once the ex-vessel transmission lines, receiver electronics, data acquisition hardware, and the 60 GHz gyrotron are developed and installed, the commissioning phase of the CTS diagnostic can commence. This phase should preferably be up to the Pre-Fusion Power Operation 2 (PFPO-2)[50] or earlier, both due to commissioning and calibration, but also to prepare to contribute to fast-ion measurements in the Fusion Power Operation (FPO) phase. The ultimate aim of the fast-ion CTS is to measure the dynamics of the fusion-born fast alphas in the FPO phase. The capability of the ITER CTS diagnostic to secure these measurements has been reviewed in this article and is described in detail in the associated references.

While the described diagnostic development of the ITER CTS system has focused on fast-ion measurements, the CTS signal carries information about a range of other ion dynamics characteristics. Examples include the bulk ion temperature, the bulk ion rotation velocity, and the fuel-ion ratio[51]. The ability of the CTS diagnostic to contribute to the measurement of these parameters depends primarily on the scattering geometry. The present ITER CTS geometry has specifically been chosen to optimize the fast-ion measurements. Nevertheless, the ITER fast-ion CTS diagnostic will be able to contribute to the determination of some of these bulk-ion features, and future studies will clarify to what extent this can be achieved.

Alternatively, one may consider strengthening the diagnostic coverage of bulk-ion measurements in ITER by installing a dedicated thermal-ion CTS system utilizing the Electron Cyclotron Resonance Heating (ECRH) system. While this is not foreseen in the original ITER diagnostic suite, it would be significantly easier to implement than most other diagnostic systems, since it can be implemented on the ECRH transmission lines in an auxiliary building at a distance from the more restricted ITER tokamak area. It would make use, synergistically, of an ECRH gyrotron and transmission lines. Proof-of-principle experiments were performed at ASDEX Upgrade (AUG) showing the potential of such a diagnostic setup[14]. As ECRH systems will be the primary external heating source for fusion prototype reactors like DEMO (EU) and STEP (UK), such an ECRH-based thermal-ion CTS system could be an important benefit to future reactors, due to the key parameter measurements and the ease of installation.

IX. ACKNOWLEDGMENTS

The work leading to this publication has been funded partially by Fusion for Energy under the Framework Partnership Agreement F4E-FPA-393. This publication reflects the views only of the author, and Fusion for Energy cannot be held responsible for any use, which may be made

of the information contained therein. The views and opinions expressed herein do not necessarily reflect those of the ITER Organization.

X. REFERENCES AND FOOTNOTES

[1]E.E. Salpeter, "Electron Density Fluctuations in a Plasma", Phys. Rev. **120**, p. 1528 (1960)
[2]H. Bindslev, "A quantitative study of scattering from electromagnetic fluctuations in plasmas", J. Atmos. Terr. Phys. **58** 983–989 (1996)
[3]S.B. Korsholm et al, "Collective Thomson scattering capabilities to diagnose fusion plasmas", Nucl. Instrum. Methods Phys. Res. **623**, pp. 677-680 (2010)
[4]R. Behn, et al., "Ion temperature measurement of tokamak plasmas by collective Thomson scattering of D_2O laser radiation", Phys. Rev. Lett. **62** p. 2833 (1989)
[5]E.V. Suvorov et al., "Ion temperature and beam-driven plasma waves from collective scattering of gyrotron radiation in W7-AS", Plasma Phys. Control. Fusion **37**, p. 1207 (1995)
[6]J.A. Hoekzema et al., "First results of collective scattering on JET (invited)", Rev. Sci. Instrum. **68**, 275 (1997)
[7]H. Bindslev, J.A. Hoekzema, J. Egedal, J.A. Fessey, T.P. Hughes, J.S. Machuzak, "Fast-ion velocity distributions in JET measured by collective thomson scattering", Phys. Rev. Lett. **83**, 3206 (1999)
[8]H. Bindslev et al., "Fast-Ion Dynamics in the TEXTOR Tokamak Measured by Collective Thomson Scattering", Phys. Rev. Lett. **97**, 205005 (2006)
[9]S.B. Korsholm et al, "Current fast ion collective Thomson scattering diagnostics at TEXTOR and ASDEX Upgrade, and ITER plans (invited)", Rev. Sci. Instrum. **77**, 10E514 (2006)
[10]M. Stejner et al., "Temporally resolved plasma composition measurements by collective Thomson scattering in TEXTOR", Rev. Sci. Instrum, **83**, 10E307 (2012)
[11]S.K. Nielsen et al, "Recent development of collective Thomson scattering for magnetically confined fusion plasmas", Phys. Scr. **92**, 024001 (2017)
[12]F. Meo et al., "Commissioning activities and first results from the collective Thomson scattering diagnostic on ASDEX Upgrade (invited)", Rev. Sci. Instrum. **79**, 10E501 (2008)
[13]Salewski et al., "Comparison of fast ion collective Thomson scattering measurements at ASDEX Upgrade with numerical simulations", Nucl. Fusion **50**, 035012 (2010)
[14]M. Stejner et al., "Main-ion temperature and plasma rotation measurements based on scattering of electron cyclotron heating waves in ASDEX Upgrade", Plasma Phys. Control. Fusion **59** 075009 (2017)
[15]S.K. Nielsen et al., "Measurements of the fast-ion distribution function at ASDEX upgrade by collective Thomson scattering (CTS) using active and passive views", Plasma Phys. Control. Fusion **57**, 035009 (2015)
[16]W. Bin et al., "Advances in the FTU collective Thomson scattering system", Rev. Sci. Instrum. **87**, 11E507 (2016)
[17]S. Kubo et al., "Collective Thomson scattering of a high power electron cyclotron resonance heating beam in LHD", Rev. Sci. Instrum **81**, 10D535 (2010)
[18]M. Nishiura et al., "Spectrum response and analysis of 77 GHz band collective Thomson scattering diagnostic for bulk and fast ions in LHD plasmas", Nucl. Fusion **54**, 023006 (2014)
[19]D. Moseev et al, "Collective Thomson scattering diagnostic at Wendelstein 7-X", Rev. Sci. Instrum. **90**, 013503 (2019)
[20]W.C. Deng et al, "Development of a 105 GHz fast ion collective Thomson scattering diagnostic on HL-2A tokamak", J. Inst. **17**, C02006 (2022)
[21]S.B. Korsholm et al, "Measurements of Intrinsic Ion Bernstein Waves in a Tokamak by Collective Thomson Scattering", Phys. Rev. Lett. **106** 165004 (2011)
[22]M. Stejner, S.K. Nielsen, H. Bindslev, S.B. Korsholm, M. Salewski, "Principles of fuel ion ratio measurements in fusion plasmas by collective Thomson scattering", Plasma Phys. Control. Fusion **53** 065020 (2011)
[23]European Fusion Development Agreement
[24]H. Bindslev, F. Meo, E.L. Tsakadze, S.B. Korsholm, P. Woskov, "Feasibility study of fast ion diagnosis in ITER by collective Thomson scattering, millimeter waves to CO2 laser", Rev. Sci. Instrum, **75**, 3598 (2004)
[25]F. Meo, H. Bindslev, S.B. Korsholm, E.L. Tsakadze, C.I. Walker, P. Woskov, G. Vayakis, "Design of the collective Thomson scattering diagnostic for International Thermonuclear Experimental Reactor at the 60 GHz frequency range", Rev. Sci. Instrum. **75**, 3585 (2004)
[26]F. Leipold et al., "Antenna design for fast ion collective Thomson scattering diagnostic for the international thermonuclear experimental reactor", Rev. Sci. Instrum. **80**, 093501 (2009)
[27]M. Salewski et al., "Comparison of collective Thomson scattering signals due to fast ions in ITER scenarios with fusion and auxiliary heating", Plasma Phys. Control. Fusion **51**, 035006 (2009)
[28]M. Salewski, L.-G. Eriksson, H. Bindslev, S.B. Korsholm, F. Leipold, F. Meo, P. Michelsen, S.K. Nielsen, "Impact of ICRH on the measurement of fusion alphas by collective Thomson scattering in ITER", Nucl. Fusion **49**, 025006 (2009)
[29]M. Salewski et al., "On velocity space interrogation regions of fast-ion collective Thomson scattering at ITER", Nucl. Fusion **51**, 083014 (2011)
[30]Consortium of Technical University of Denmark (DTU) and Instituto Superior Técnico (IST)
[31]F4E-FPA-393 Framework Partnership Agreement on Diagnostic Development and Design: LFS CTS
[32]S.B. Korsholm et al., "Design and development of the ITER CTS diagnostic", EPJ Web Conf. **203**, p. 03002 (2019)
[33]J. Rasmussen et al., "Modelling the electron cyclotron emission below the fundamental resonance in ITER", Plasma Phys. Control. Fusion **61**, 095002 (2019)
[34]A.W. Larsen et al, "Mitigation of EC breakdown in the gyrotron transmission line of the ITER Collective Thomson Scattering diagnostic via a Split Biased Waveguide", J. Inst. **14**, C11009 (2019)
[35]C.P. Moeller, R. Prater, A.C. Riviere, N.R.G. Ainsworth, A.N. Dellis, P.C. Johnson, "A High Field Launch for Electron Cyclotron Heating using an External Window", Plasma Physics and Fusion Technology (A1411), EC-6, p. 355-360 (1987)
[36]J. Trieschmann, A.W. Larsen, T. Mussenbrock, S.B. Korsholm, "Kinetic simulation of electron cyclotron resonance assisted gas breakdown in split-biased waveguides for ITER collective Thomson scattering diagnostic", Phys. Plasmas **28**, 082505 (2021)
[37]J. Rasmussen, M. Stejner, T. Jensen, E.B. Klinkby, S.B. Korsholm, A.W. Larsen, F. Leipold, S.K. Nielsen, M. Salewski, "Inference of α-particle density profiles from ITER collective Thomson scattering", Nucl. Fusion **59**, 096051 (2019)
[38]M. Salewski et al, "Alpha-particle velocity-space diagnostic in ITER", Nucl. Fusion **58**, 096019 (2018)
[39]M. Nocente et al, "Conceptual design of the radial gamma ray spectrometers system for α particle and runaway electron measurements at ITER", Nucl. Fusion **57**, 076016 (2017)
[40]M. Salewski, "Diagnostic of fast-ion energy spectra and densities in magnetized plasmas", J. Inst. **14**, C05019 (2019)
[41]A. Lopes et al, "Neutronics analysis of the ITER Collective Thomson Scattering system", Fus. Eng. Des. **134**, pp. 22-28 (2018)
[42]A. Lopes et al, "Shielding analysis of the ITER Collective Thomson Scattering system", Fus. Eng. Des. **161**, pp. 111994 (2020)
[43]A. Chambon et al, "Assessment of shutdown dose rates in the ITER Collective Thomson Scattering system and in equatorial port plug 12", J. Inst. **16**, C12001 (2021)
[44]C. Vidal et al, "Thermo-structural analyses of the in-vessel components of the ITER collective Thomson scattering system", Fus. Eng Des. **140**, pp. 123-132 (2019)
[45]V. Infante et al, "RAMI analysis of the ITER LFS CTS system", Fus. Eng Des. **123**, pp. 663-668 (2017)
[46]D. Rechena, V. Infante, E. Henriques, S.B. Korsholm, A.W. Larsen, B. Gonçalves, A. Vale, R. Luis, "RAMI analysis of the collective Thomson scattering system front-end – Part1 – Failure modes effects and criticality analysis", Fus. Eng Des. **168**, pp. 112454 (2021)
[47]D. Rechena, V. Infante, E. Henriques, S.B. Korsholm, A.W. Larsen, B. Gonçalves, A. Vale, R. Luis, "RAMI analysis of the collective Thomson scattering system front-end – Part2 – reliability block diagram analysis", Fus. Eng Des. **171**, pp. 112593 (2021)
[48]ITER Remote Maintenance Management System, ITER_D_2FMAJY
[49]S.B. Korsholm, F. Leipold, R.B. Madsen, H. Gutierrez, T. Jensen, M. Jessen, A.W. Larsen, J. Rasmussen, M. Salewski, "Fast production of microwave component prototypes by additive manufacturing and copper coating", Rev. Sci. Instrum. **92** pp. 033509 (2021)
[50]ITER Research Plan within the Staged Approach, ITR-18-003
[51]M. Stejner et al., "The prospect for fuel ion ratio measurements in ITER by collective Thomson scattering", Nucl. Fusion **52**, 023011 (2012)

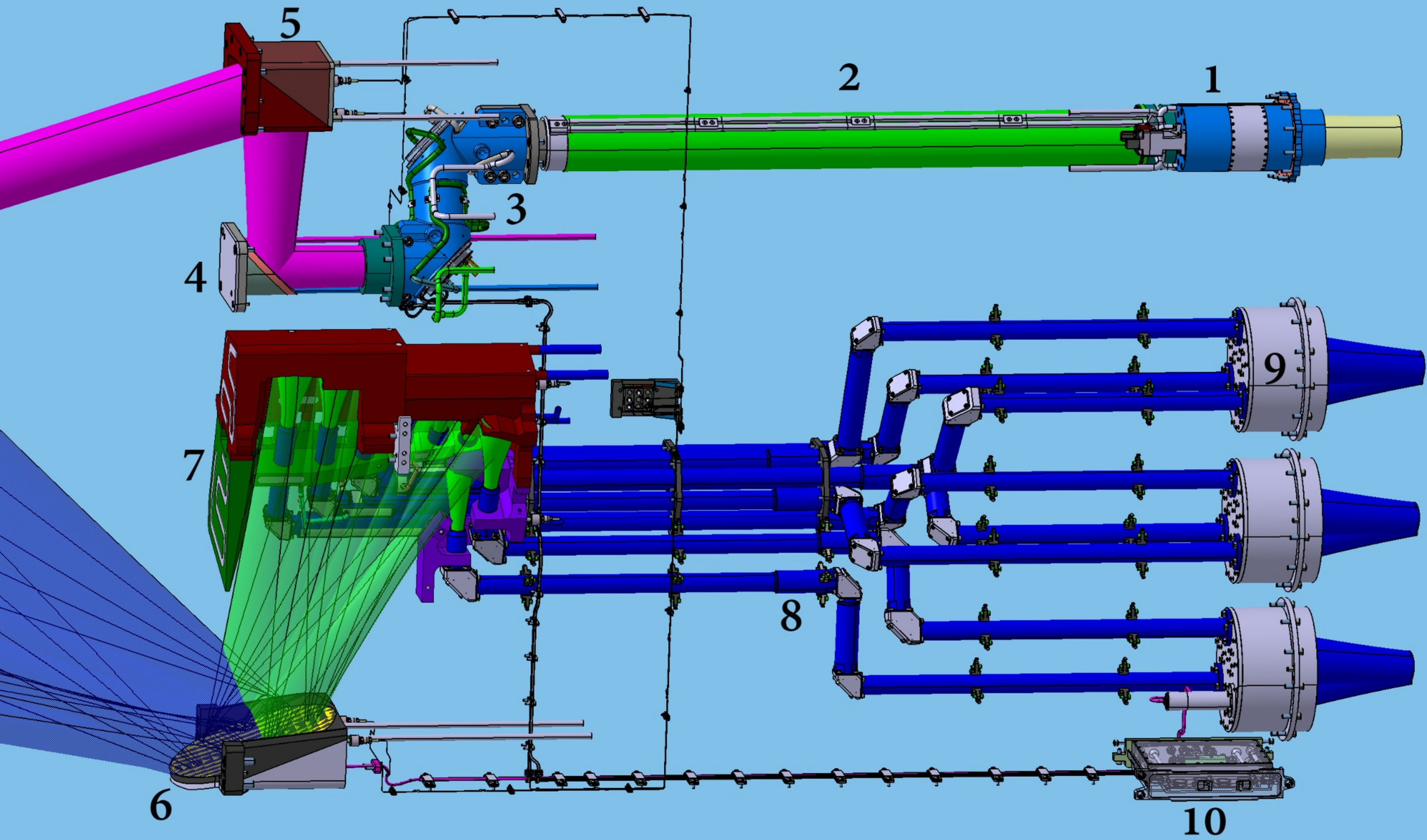
5
2
1
3
4
9
7
8
6
10

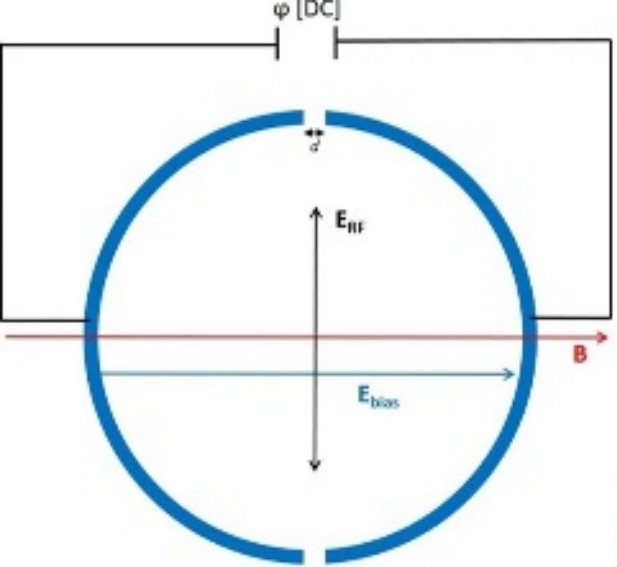
φ [DC]
d
E_RF
B
E_bias

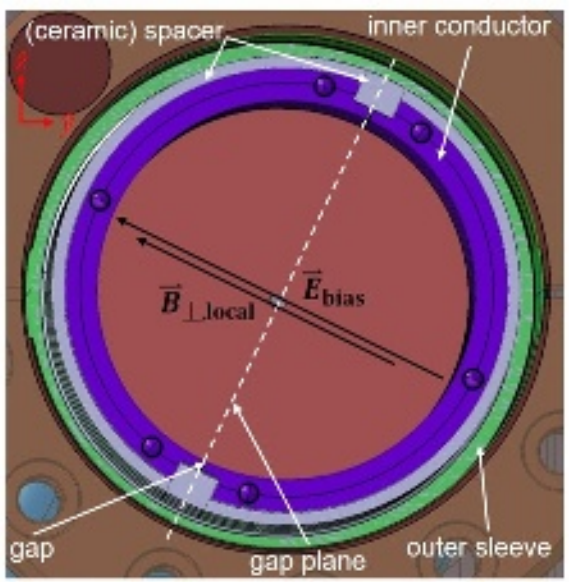
(ceramic) spacer
inner conductor
$\vec{B}_{\perp local}$
$\vec{E}_{bias}$
gap
gap plane
outer sleeve

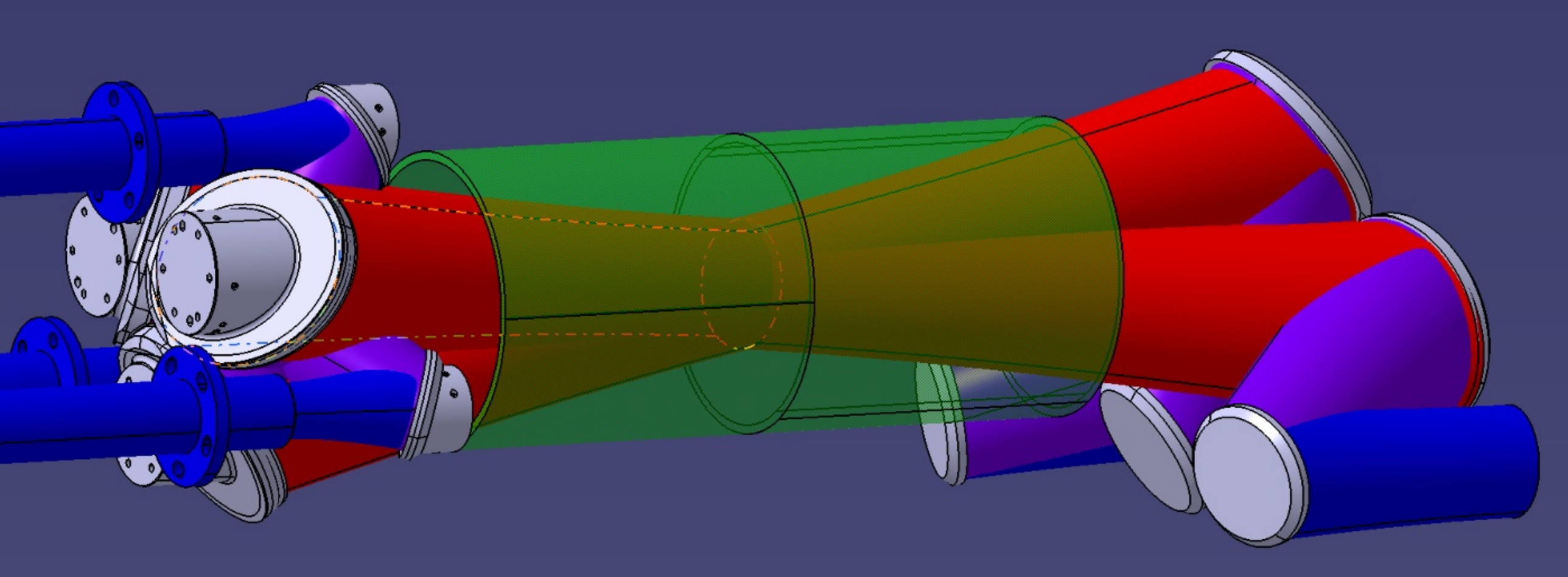

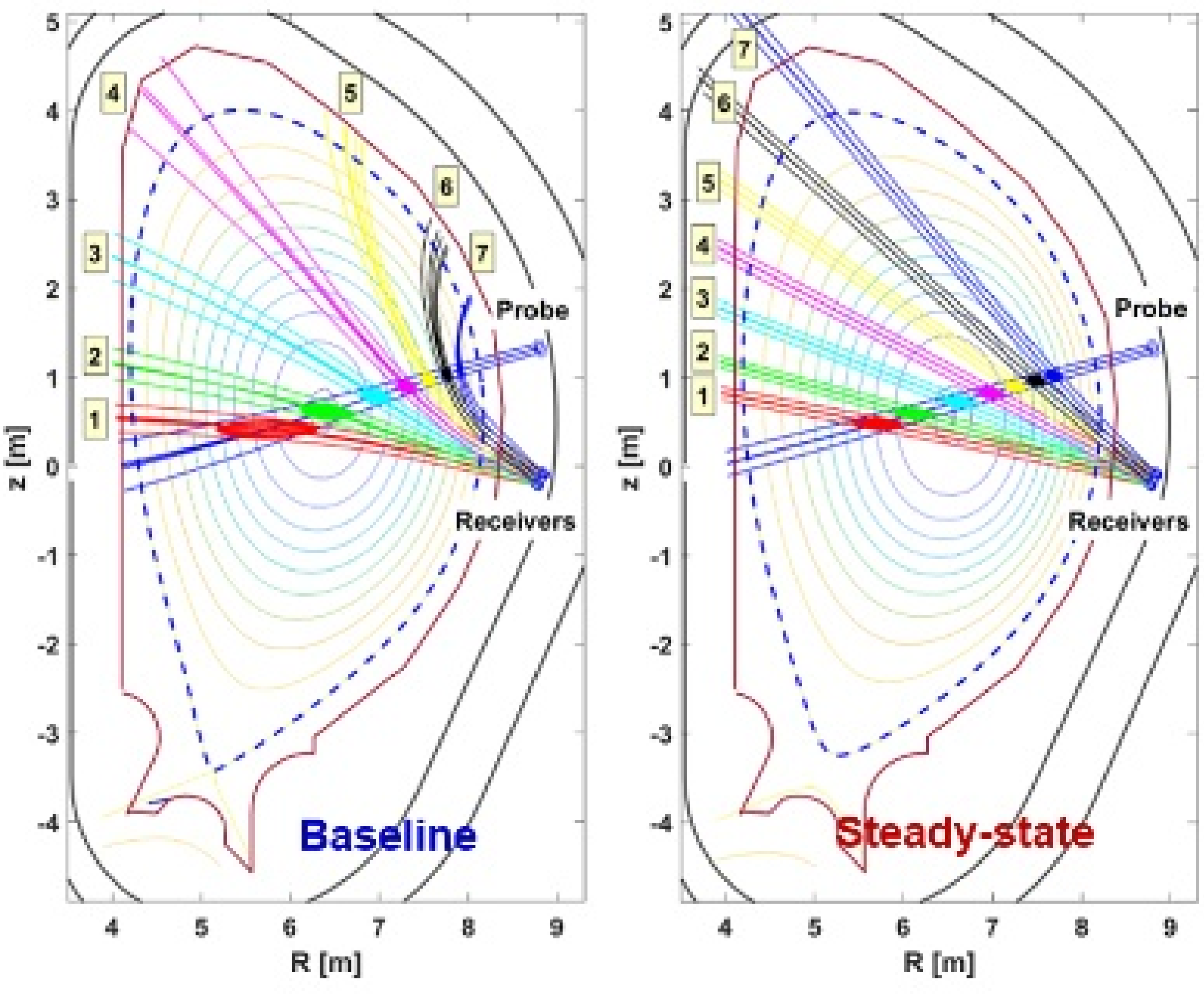
Baseline
Steady-state
Probe
Receivers
R [m]
z [m]

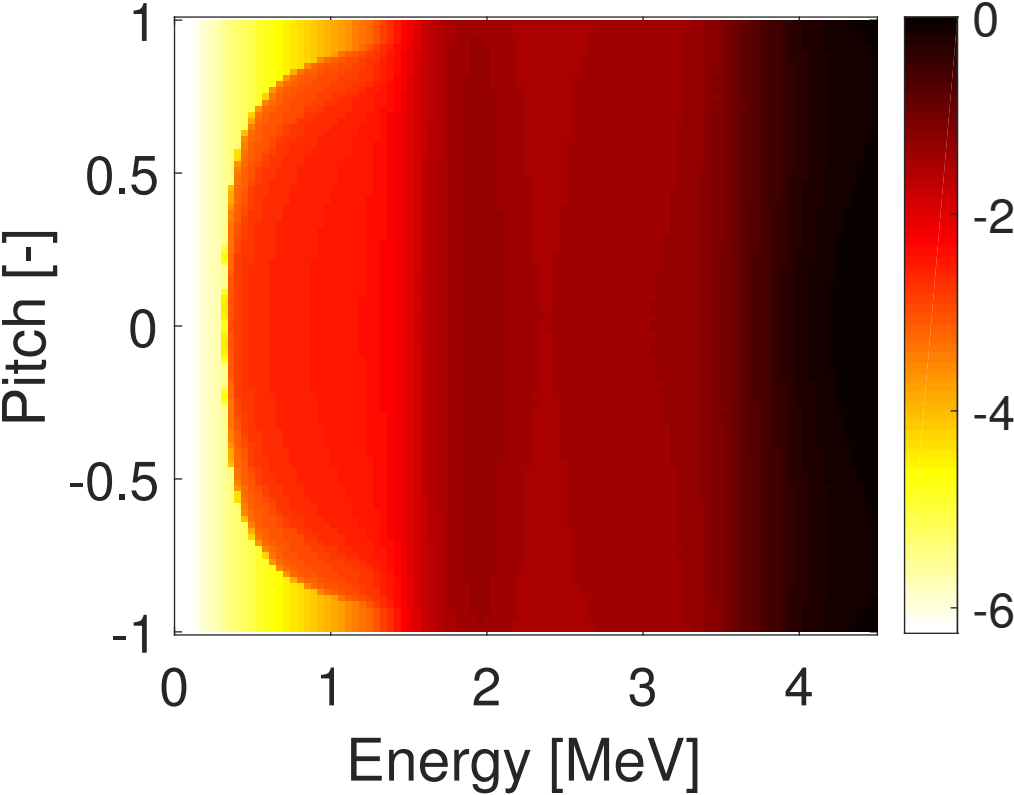
1
0.5
0
-0.5
-1
Pitch [-]
0
1
2
3
4
Energy [MeV]
0
-2
-4
-6